A Highly-Accurate Industrial Robot Calibrator with Multi-Planer Constraints Supplementary Material

Anonymous

This is the supplementary file for the paper, where the convergence proof of the AMPC algorithm is provided. Moreover, additional tables and figures regarding the symbol appointment, model parameters, experimental process and results and the MCS-AMPC's pseudocode are placed here.

I. Additional Tables

TABLE S.I. Symbol list.

Symbol	Explanation
$\mathbb{R}_i$	Transformation matrix.
a, θ, α, d	Link length, joint angle, link twist angle, link offset.
H, S	Nominal position matrix, Nominal rotation vector.
$\Delta\mathbb{R}$, $\mathbb{R}_r$, $\mathbb{R}$	Pose deviation, actual pose matrix, nominal pose matrix
A	Jacobian matrix of the error model.
$\Delta\xi$	Kinematic parameters error vector.
$\Delta\alpha$, Δa, Δd ,$\Delta\theta$	Vector of the kinematic parameter deviations.
M	Sample count (measurement configurations).
C, $\hat{C}$	Cable measured length, cable nominal length.
S_0	Fixed point coordinate on the ground.
S_i	Nominal position coordinate.
$\{q_{i,1}, \ldots, q_{i,6}\}$	Torsion angles.
f	Objective function.
$\hat{A}$	Error extended Jacobian matrix.
Z, $\hat{Z}$	Orthogonal matrices.
Λ	Diagonal matrix.
z	Dimension of the D-H parameter vector.
$(\sigma_1, \sigma_2, \cdots, \sigma_z)$	Singular values of the matrix Λ.
$O_1, \ldots, O_6$,	Observability indices
m	Selected sample count (measurement configurations selected by MCS)
u	D-H parameter vector.
Λ_k	Regularized constant.
a_6	Link length of the robot's sixth axis.
$\hat{a}_6$	Defined link length of the robot's sixth axis.
D	Length of the dial indicator.
$\hat{D}$	Dial indicator reading.
ψ_k	Constraint equation of plane k.
G_k	A point of plane k.
η_j	Normal vector of plane k.
n	Total number of planes.
ρ_k	Constraint factor for plane k.
Υ_k	Lagrange multiplier of plane k.
$<\cdot>$	Inner product between two matrices.
I	Unit matrix.
l_k	Distance from the point on the plane k to the industrial robot coordinate origin.
τ_k	Step size of the Lagrange multiplier of the plane k.
a_1	An element of w.
B_i	Measured position.
K_1, K_2, K_3	Max iteration's round.

TABLE S.II. HRS JR680 industrial robot D-H parameters.

No.	a_i/mm	θ_i/°	α_i/°	d_i/mm
Joint 1	250	0	-90	653.5
Joint 2	900	-90	0	0
Joint 3	-205	180	-90	0
Joint 4	0	0	90	1030.2
Joint 5	0	90	-90	0
Joint 6	0	0	0	200.6

TABLE S.III. CALIBRATION ACCURACY OF ALGORITHMS M1-9 ON P1-3.

Algorithms	P1			P2			P3		
	RMSE/mm	MEAN/mm	MAX/mm	RMSE/mm	MEAN /mm	MAX/mm	RMSE/mm	MEAN /mm	MAX/mm
Before	2.56	2.45	4.51	2.56	2.45	4.51	2.56	2.45	4.51
M1	$0.979_{\pm 5.2E-2}$	$0.878_{\pm 4.8E-2}$	$1.755_{\pm 4.9E-2}$	$0.930_{\pm 3.6E-2}$	$0.824_{\pm 3.2E-2}$	$1.702_{\pm 2.9E-2}$	$0.921_{\pm 2.2E-2}$	$0.803_{\pm 2.2E-2}$	$1.686_{\pm 2.8E-2}$
M2	$1.252_{\pm 3.3E-2}$	$1.162_{\pm 3.8E-2}$	$2.425_{\pm 6.5E-2}$	$1.195_{\pm 9.1E-3}$	$1.108_{\pm 1.0E-2}$	$2.375_{\pm 1.1E-2}$	$1.182_{\pm 3.2E-2}$	$1.066_{\pm 3.1E-2}$	$2.293_{\pm 5.5E-2}$
M3	$0.653_{\pm 0.5E-0}$	$0.573_{\pm 0.3E-0}$	$1.125_{\pm 0.6E-0}$	$0.601_{\pm 0.2E-2}$	$0.510_{\pm 0.7E-2}$	$1.094_{\pm 0.3E-2}$	$0.587_{\pm 0.2E-2}$	$0.503_{\pm 0.6E-2}$	$1.035_{\pm 0.1E-2}$
M4	$0.772_{\pm 5.9E-3}$	$0.673_{\pm 5.9E-3}$	$1.522_{\pm 5.0E-2}$	$0.712_{\pm 4.0E-2}$	$0.612_{\pm 4.0E-2}$	$1.460_{\pm 5.1E-2}$	$0.673_{\pm 4.6E-2}$	$0.572_{\pm 3.8E-2}$	$1.406_{\pm 5.3E-2}$
M5	$1.068_{\pm 4.0E-2}$	$0.887_{\pm 3.9E-2}$	$1.858_{\pm 3.2E-2}$	$1.030_{\pm 2.8E-2}$	$0.818_{\pm 3.1E-2}$	$1.808_{\pm 3.2E-2}$	$1.023_{\pm 3.2E-2}$	$0.812_{\pm 3.3E-2}$	$1.793_{\pm 6.9E-2}$
M6	$0.698_{\pm 1.3E-0}$	$0.597_{\pm 1.1E-0}$	$1.321_{\pm 1.0E-0}$	$0.643_{\pm 5.2E-3}$	$0.541_{\pm 2.8E-3}$	$1.279_{\pm 2.2E-2}$	$0.629_{\pm 2.0E-2}$	$0.525_{\pm 7.1E-3}$	$1.255_{\pm 1.6E-2}$
M7	$1.111_{\pm 5.8E-2}$	$1.012_{\pm 4.9E-2}$	$2.101_{\pm 6.3E-2}$	$1.060_{\pm 5.3E-2}$	$0.965_{\pm 4.9E-2}$	$2.054_{\pm 5.0E-2}$	$1.052_{\pm 4.0E-2}$	$0.950_{\pm 3.2E-2}$	$2.030_{\pm 5.2E-2}$
M8	$0.594_{\pm 1.9E-2}$	$0.492_{\pm 1.8E-2}$	$0.965_{\pm 1.9E-2}$	$0.565_{\pm 1.9E-2}$	$0.465_{\pm 1.8E-2}$	$0.913_{\pm 1.9E-2}$	$0.551_{\pm 5.8E-2}$	$0.451_{\pm 4.0E-2}$	$0.890_{\pm 4.0E-2}$
M9	$0.549_{\pm 1.8E-2}$	$0.449_{\pm 1.6E-2}$	$0.885_{\pm 1.9E-2}$	$0.528_{\pm 0.9E-0}$	$0.423_{\pm 0.8E-0}$	$0.829_{\pm 0.6E-0}$	$\mathbf{0.502_{\pm 0.2E-0}}$	$\mathbf{0.411_{\pm 0.3E-0}}$	$\mathbf{0.815_{\pm 0.2E-0}}$

TABLE S.IV. TOTAL TIME COSTS OF ALGORITHMS M1-9 ON P1-3.

Datasets	Items	M1	M2	M3	M4	M5	M6	M7	M8	M9
P1	Iteration	26	12	50	85	16	65	13	11	2
	Time/s	$75.2_{\pm 0.53}$	$22.0_{\pm 1.72}$	$108.0_{\pm 0.26}$	$42.1_{\pm 0.82}$	$30.0_{\pm 3.12}$	$122.6_{\pm 0.32}$	$19.0_{\pm 0.10}$	$22.73_{\pm 0.83}$	$43.31_{\pm 0.11}$
P2	Iteration	25	12	49	82	16	65	13	11	2
	Time/s	$130.10_{\pm 0.93}$	$42.05_{\pm 1.02}$	$192.61_{\pm 1.06}$	$80.86_{\pm 2.02}$	$59.22_{\pm 3.69}$	$228.52_{\pm 0.53}$	$38.85_{\pm 0.53}$	$42.62_{\pm 1.20}$	$54.19_{\pm 0.23}$
P3	Iteration	23	12	49	79	15	63	12	10	**2**
	Time/s	$202.1_{\pm 1.21}$	$65.2_{\pm 1.02}$	$289.3_{\pm 0.99}$	$120.2_{\pm 3.89}$	$82.16_{\pm 3.52}$	$328.63_{\pm 0.59}$	$63.6_{\pm 0.38}$	$65.3_{\pm 1.98}$	$\mathbf{62.8_{\pm 0.23}}$

TABLE S.V. WILCOXON SIGNED RANKS TEST ON RMSE/MEAN/MAX OF TABLE S. III.

Comparison	*R-*	*R+*	*p-value*
M9 vs. M1	0	45	0.002
M9vs. M2	0	45	0.002
M9 vs. M3	0	45	0.002
M9 vs. M4	0	45	0.002
M9 vs. M5	0	45	0.002
M9 vs. M6	0	45	0.002
M9 vs. M7	0	45	0.002
M9 vs. M8	0	45	0.002

*Highlighted are the hypotheses that are accepted at a significance level of 0.05.

TABLE S.VI. THE D-H PARAMETERS DEVIATIONS ON P1-3 AFTER CALIBRATION BY M9.

	P1				P2				P3			
No.	Δa_i/°	Δa_i/mm	Δd_i/mm	$\Delta \theta_i$/°	Δa_i/°	Δa_i/mm	Δd_i/mm	$\Delta \theta_i$/°	Δa_i/°	Δa_i/mm	Δd_i/mm	$\Delta \theta_i$/°
Joint 1	-0.2135	-0.2361	0.5693	0.0261	-0.3135	-0.2671	0.7635	0.0163	-0.2133	-0.1125	0.8120	0.0157
Joint 2	-0.0335	-2.3652	-0.3629	-0.0987	-0.0135	-2.1051	-0.5378	-0.0537	-0.0156	-2.1631	-0.6389	-0.0535
Joint 3	0.1568	1.3658	-0.3268	0.0571	0.0968	1.3328	-0.2253	0.0885	0.0245	1.3552	-0.2377	0.0862
Joint 4	-0.0345	0.8369	1.8435	0.0588	-0.0145	0.5371	2.0040	0.0679	-0.0035	0.6372	2.2214	0.0653
Joint 5	0.0261	-0.3261	0.5879	0.0196	0.0661	-0.2162	0.3222	0.0035	0.0357	-0.2672	0.3221	0.0032
Joint 6	0.1203	-0.1578	-0.5326	0.0063	0.1155	-0.0988	-0.5738	0.0027	0.0965	-0.0681	-0.5737	0.0026

II. ADDITIONAL ALGORITHM PSEUDOCODE

Algorithm I: MCS-AMPC Calibrator

Input: w_0, z, K_1, K_2, K_3, M, $\{q_{i,1}, q_{i,2}, \ldots, q_{i,6}\}$, $\{C_1, C_2, \ldots, C_M\}$, $G_{0,k}$, $\eta_{0,k}$, $\Upsilon_{0,k}$, n, S_0

Operation	**Cost**
/* Initialization */	
1. **initialize** n=3, λ_k, v=2, ρ_k	T_1
2. **initialize** w=w_0, G_k=$G_{0,k}$, η_k=$\eta_{0,k}$, Υ_k=$\Upsilon_{0,k}$, S_0	
/* MCS Step*/	
3. **for** t= z to N_0	
4. g=t	
5. **calculate** O_6 via **Algorithm II**	
6. **end for**	
7. **output** m according to the observability indices	
8. **for** t_1=1 to K_1	T_2
9. **generate** m configurations randomly from M configurations	
10. s=m	
11. **calculate** O_6 via **Algorithm II**	
12. **building** the MCS based on the updated rules of the DE algorithm	
13. **end for**	
Output m measurement configurations (a best group of samples)	
/* AMPC Step */	
Input a best group of samples	
21. **for** t_2=1 to K_2	
22. **for** i=1 to m	
23. **update** $S_{0,t+1}$ with (17)	
25. **end for**	
26. **end for**	
27. **for** t_3=1 to K_3	
28. **for** i=1 to m	T_3
29. **update** $G_{k,t+1}$, and $\eta_{k,t+1}$ with (18) and (19)	
30. **update** w_{t+1} with (21)	
31. **update** $\Upsilon_{j,t+1}$ with (22)	
32. **normalize** $G_{j,t+1}$, and $\eta_{j,t+1}$ with (20)	
33. **end for**	
34. **end for**	
/* Operation Ending */	
Output: w	

Algorithm II: Calculation of O_6

Input: w_0, g, $\{q_{i,1}, q_{i,2}, \ldots, q_{i,6}\}$,

Operation	**Cost**
/* Initialization */	
1. **Initialize** u=u_0, g	T_{21}
/*MCS Step*/	
2. **for** i=1 to g	
3. **calculate** the A with (5)	
4. **end for**	
5. **computing** $\hat{A}$ based on (8)	T_{22}
6. **update** σ_1-σ_z with (9) and (10)	
7. **updating** O_6 based on (11)	
/* Operation Ending */	
Output: O_6	

III. ADDITIONAL FIGURES

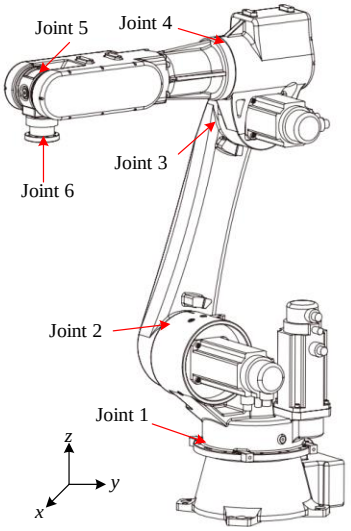

Fig. S.1. The HSR-JR680 industrial robot. The picture originates from this website (https://www.hsrobotics.cn/download.php).

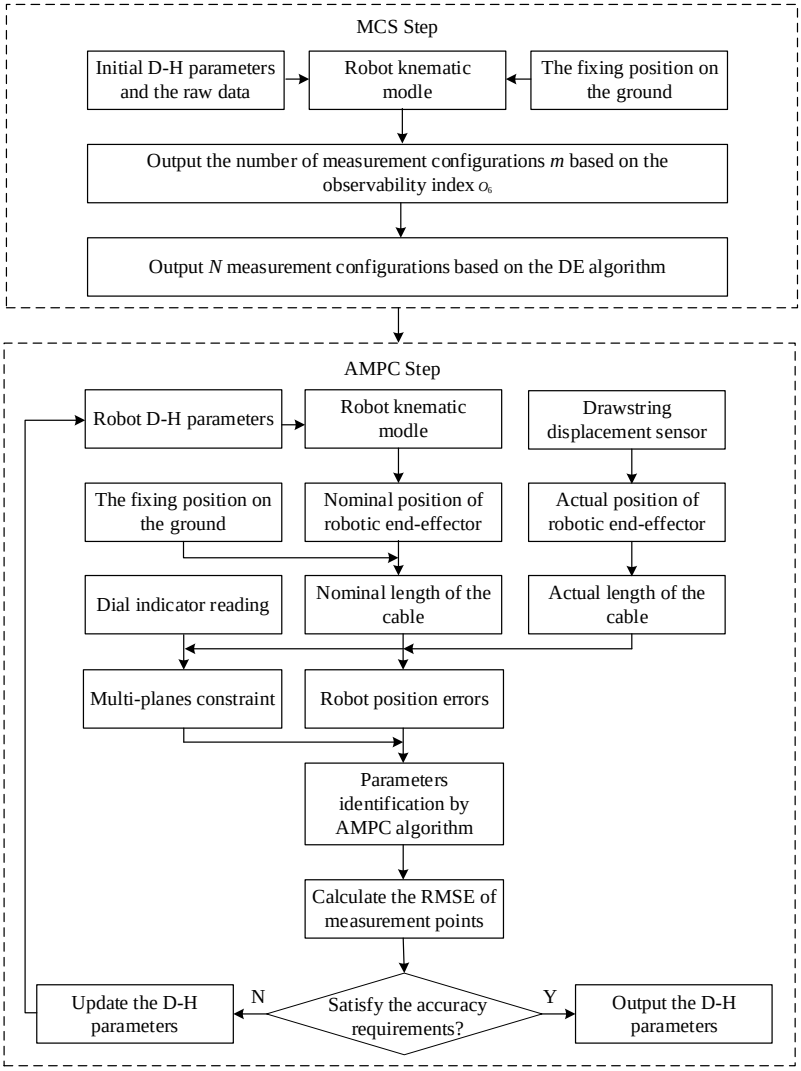

Fig. S.2. The calibration process for the industrial robot.

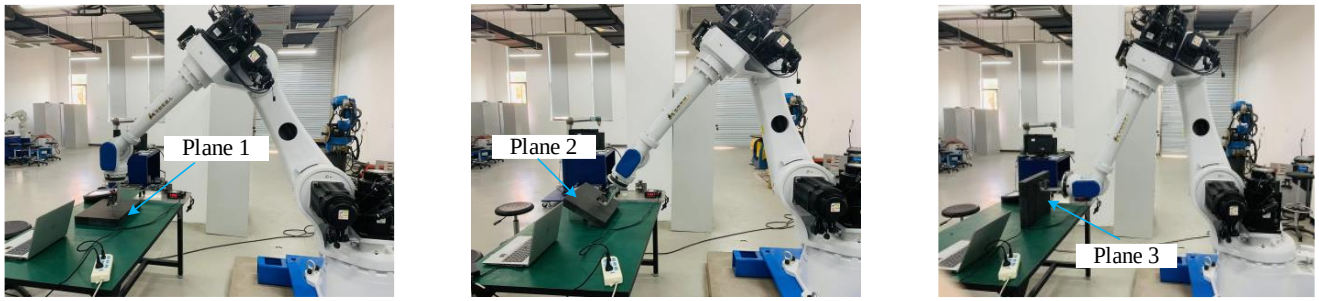

(a) (b) (c)

Fig. S.3. The samples collection process on D1-3. (a), (b) and (c) are corresponded to D1-3, respectively.

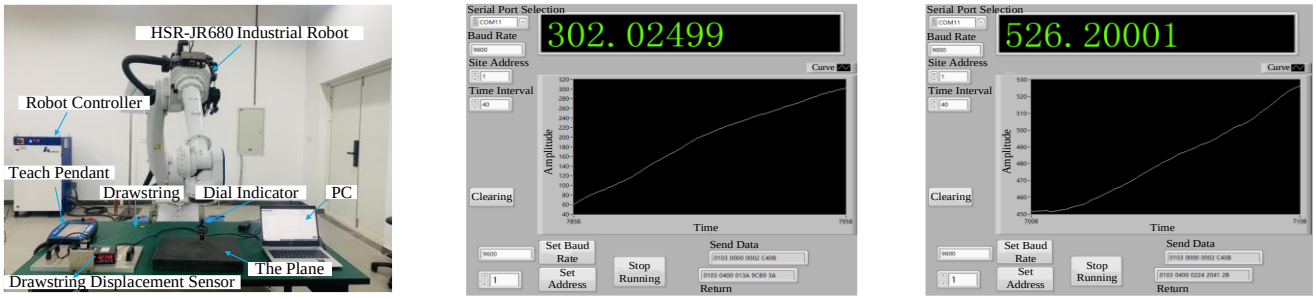

(a) (b) (c)

Fig. S.4. The experimental system. (a) The experimental platform, (b) and (c) The LabVIEW software on two different samples.

(a) (b) (c)

Fig. S.5. The experimental process. (a), (b) and (c) depict three various measurement positions on D1.

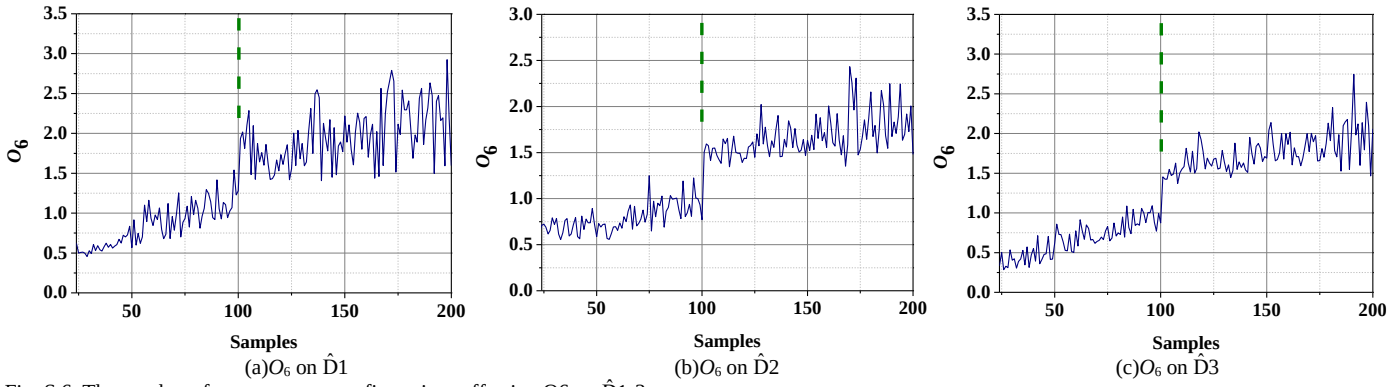

(a)O_6 on $\hat{D}1$ (b)O_6 on $\hat{D}2$ (c)O_6 on $\hat{D}3$

Fig. S.6. The number of measurement configurations affecting O6 on $\hat{D}1$-3.

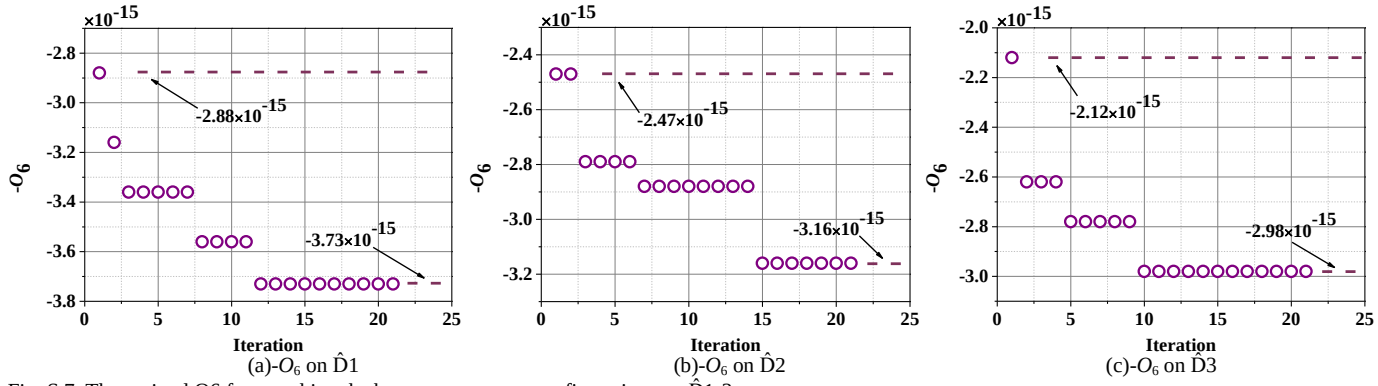

(a)-O_6 on $\hat{D}1$ (b)-O_6 on $\hat{D}2$ (c)-O_6 on $\hat{D}3$

Fig. S.7. The optimal O6 for searching the best measurement configurations on $\hat{D}1$-3.

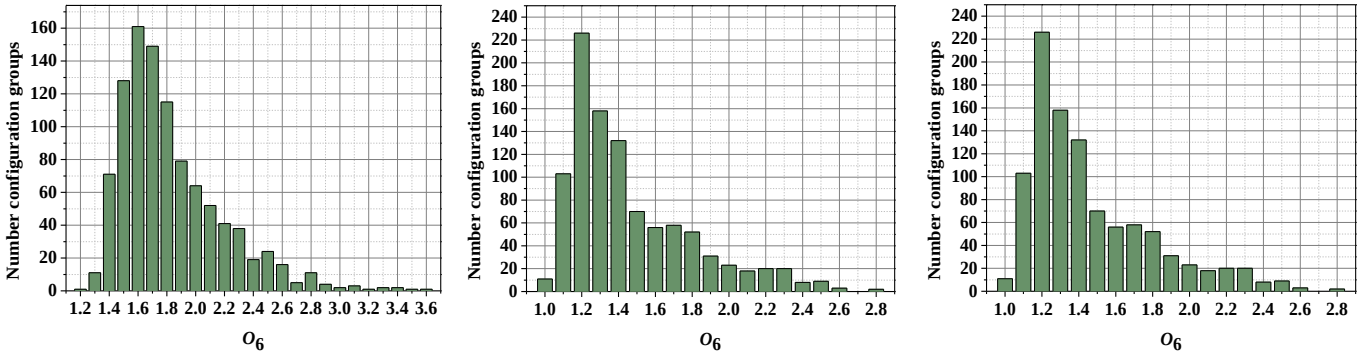

(a) (b) (c)

Fig. S.8. The distributions of the observability indices are calculated 1000 times on $\hat{D}1$-3. This experimental propose is to randomly select 100 measurement configurations in 200 samples.

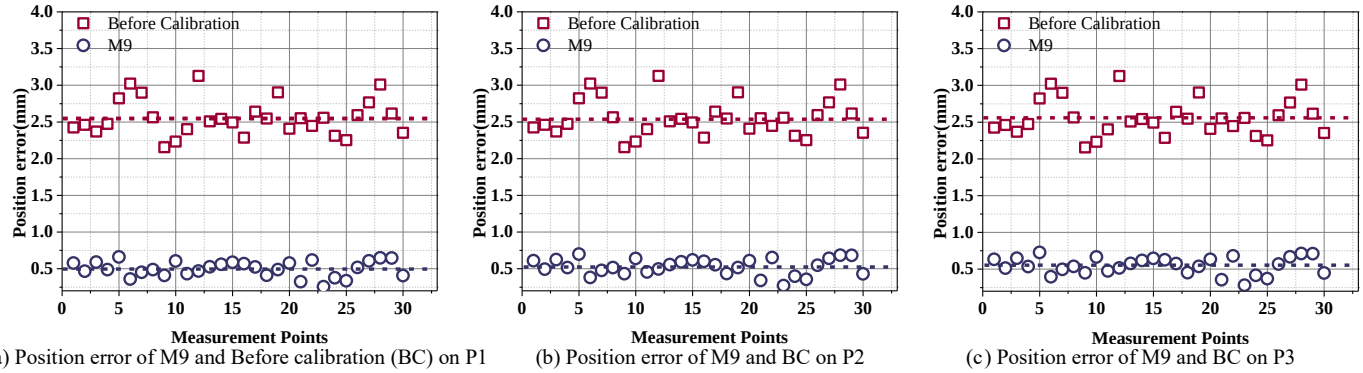

(a) Position error of M9 and Before calibration (BC) on P1 (b) Position error of M9 and BC on P2 (c) Position error of M9 and BC on P3

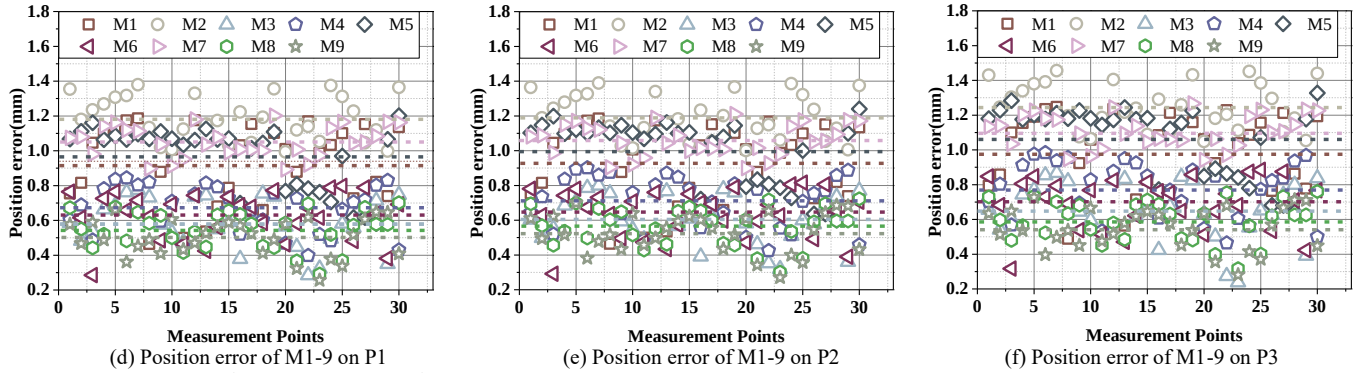

(d) Position error of M1-9 on P1 (e) Position error of M1-9 on P2 (f) Position error of M1-9 on P3

Fig. S.9. The position error of the industrial robot after calibration using various algorithms on P1-3. Note that the dotted lines represent the average values. Panels (a)-(c) illustrate that the industrial robot obtains an evident enhancement of position accuracy after calibration. Panels (d)-(f) show that M9 has the best position accuracy when compared to M1-8.

IV. Convergence Analysis of AMPC

Given nodes $i \in m$, and iteration t, the convergence is divided into two sequential steps:
Step 1. The difference between Υ_{t+1} and Υ_t is bounded by that between (η_{t+1}, G_{t+1}, $a_{1,t+1}$) and (η_t, G_t, $a_{1,t}$);
Step 2. The augmented Lagrangian function (23) is non-increasing and low-bounded.

A. Proof of Step 1

This work provides proof with Γ as an active variable. Thus, *Lemma* 1 is presented as:
Lemma 1: With (29), $(\Upsilon_{t+1}\text{-}\Upsilon_t)^2$ is bounded by:

$$\left(\Upsilon_{t+1}-\Upsilon_t\right)^2 \le 2\left(\rho\left(\tau-1\right)\right)^2\left(\frac{1}{m}\sum_{i=1}^{m}\left(\Psi_i\left(a_{t+1},G_{t+1},\eta_{t+1}\right)-\Psi_i\left(a_t,G_t,\eta_t\right)\right)\right)^2+2\left(\frac{1}{m}\sum_{i=1}^{m}\left(\frac{1}{\kappa_{2,i,t+1}}\left(a_{1,t+1}+\kappa_{1,i,t+1}\right)-\frac{1}{\kappa_{2,i,t}}\left(a_{1,t}+\kappa_{1,i,t}\right)\right)\right)^2=\nu_\Upsilon. \tag{S1}$$

Proof: Consider that (23) is non-convex, implying that any equilibrium point having a zero-gradient (e.g., a saddle point or a global/local optimum) has the potential to be a feasible solution. Given the solution to a_1 by (29c) to be $a_{1,t+1}$, yielding:

$$\Upsilon_t+\frac{1}{m}\sum_{i=1}^{m}\left(\frac{1}{\kappa_{2,i,t+1}}\left(a_{1,t+1}+\kappa_{1,i,t+1}\right)+\rho\cdot\Psi\left(a_{t+1},G_{t+1},\eta_{t+1}\right)\right)=0. \tag{S2}$$

By replacing the values of Υ derived from equations (27d) and (29d) into expression (S2), we can derive:

$$\Upsilon_{t+1}=\left(\tau-1\right)\frac{\rho}{m}\sum_{i=1}^{m}\Psi_i\left(a_{1,t+1},G_{t+1},\eta_{t+1}\right)-\frac{1}{m}\sum_{i=1}^{m}\frac{1}{\kappa_{2,i,t+1}}\left(a_{1,t+1}+\kappa_{1,i,t+1}\right)=0. \tag{S3}$$

Hence, the difference between Υ_{t+1} and Υ_t is given as:

$$\Upsilon_{t+1}-\Upsilon_t=\left(\tau-1\right)\frac{\rho}{m}\sum_{i=1}^{m}\left(\Phi_i\left(a_{1,t+1},G_{t+1},\eta_{t+1}\right)-\Phi_i\left(a_{1,t},G_t,\eta_t\right)\right)-\frac{1}{m}\sum_{i=1}^{m}\left(\frac{1}{\kappa_{2,i,t+1}}\left(a_{1,t+1}+\kappa_{1,i,t+1}\right)-\frac{1}{\kappa_{2,i,t}}\left(a_{1,t}+\kappa_{1,i,t}\right)\right). \tag{S4}$$

With the inequality $(x\text{-}y)^2 \le 2(x^2+y^2)$, (S1) is fulfilled. Thus, *Lemma* 1 stands to implement Step 1.

B. Proof of Step 2

To facilitate the execution of Step 2, we present *Lemma* 2:
Lemma 2: If the following criteria are fulfilled:

$$\rho\le 0,\ \tau\ge 0,\ \eta_{x,t}\ge 0,\ \eta_{y,t}\ge 0,\ \eta_{z,t}\ge 0, \tag{S5a}$$

$$\frac{1}{\kappa_{2,i,t+1}}\left(a_{1,t+1}+\kappa_{1,i,t+1}\right)\le 0,\ \tau\ge\frac{1}{2}, \tag{S5b}$$

the following inequality stands:

$$f\left(\eta_{t+1},G_{t+1},a_{1,t+1},\Upsilon_{t+1}\right)-f\left(\eta_t,G_t,a_{1,t},\Psi_t\right)\le 0, \tag{S6a}$$

$$f\left(\eta_{t+1},G_{t+1},a_{1,t+1},\Upsilon_{t+1}\right)\ge 0. \tag{S6b}$$

Proof: Considering the second-order Taylor expansion of f at the point of (γ_{t+1}, W_t, $a_{1,t}$ and Γ_t), we have:

$$f\left(\eta_{t+1},G_t,a_{1,t},\Upsilon_t\right)-f\left(\eta_t,G_t,a_{1,t},\Upsilon_t\right)\overset{(27a),(29a)}{=}\frac{\rho}{2m}\sum_{i=1}^{m}\begin{bmatrix}\kappa_{4,i,t}^2\left(\eta_{x,t+1}-\eta_{x,t}\right)^2+\kappa_{5,i,t}^2\left(\eta_{y,t+1}-\eta_{y,t}\right)^2\\+\kappa_{6,i,t}^2\left(\eta_{z,t+1}-\eta_{z,t}\right)^2\end{bmatrix}. \tag{S7}$$

Note that based on optimal conditions in (27a) and (29a), the first-order term is zero and has been omitted for brevity. Likewise, the difference between $f(\eta_{t+1}$, G_{t+1}, $a_{1,t}$ and $\Upsilon_t)$ and $f(\eta_{t+1}$, G_t, $a_{1,t}$ and $\Upsilon_t)$, and $f(\eta_{t+1}$, G_{t+1}, $a_{1,t+1}$ and $\Upsilon_t)$ and $f(\eta_{t+1}$, G_{t+1}, $a_{1,t}$ and $\Upsilon_t)$ can be formulated by:

$$f\left(\eta_{t+1},G_{t+1},a_{1,t},\Upsilon_t\right)-f\left(\eta_{t+1},G_t,a_{1,t},\Upsilon_t\right)\overset{(27b),(29b)}{=}\frac{\rho}{2m}\sum_{t=1}^{m}\left(\eta_{x,t+1}\left(G_{x,t+1}-G_{x,t}\right)^2+\eta_{y,t+1}\left(G_{y,t+1}-G_{y,t}\right)^2+\eta_{z,t+1}\left(G_{z,t+1}-G_{z,t}\right)^2\right), \tag{S8}$$

$$f\left(\eta_{t+1},G_{t+1},a_{1,t+1},\Upsilon_t\right)-f\left(\eta_{t+1},G_{t+1},a_{1,t},\Upsilon_t\right)\overset{(27c),(29c)}{=}\frac{1}{2m}\sum_{i=1}^{m}\left(1+\rho\kappa_{2,i,t}^2\right)\left(a_{1,t+1}-a_{1,t}\right)^2. \tag{S9}$$

Additionally, $f(\eta_{t+1}$, G_{t+1}, $a_{1,\,t+1}$ and $\Upsilon_{t+1})$ and $f(\eta_{t+1}$, G_{t+1}, $a_{1,\,t+1}$ and $\Upsilon_t)$ are differed as:

$$f\left(\eta_t,G_{t+1},a_{1,t+1},\Upsilon_{t+1}\right)-f\left(\eta_t,G_t,a_{1,t},\Upsilon_t\right)\overset{(27d),(29d)}{=}\frac{\left(\Upsilon_{t+1}-\Upsilon_t\right)^2}{\tau\rho}\overset{S1}{\le}\frac{\nu_\Upsilon}{\tau\rho}. \tag{S10}$$

With (S9), the equality can be deduced from the update rules (27d) and (29d), whereas the inequality is contingent upon the premises established in Lemma 1. Through a logical combination of equations (S7) to (S10), the following result can be inferred:

$$
\begin{aligned}
&f\left(\eta_t, G_{t+1}, a_{1,t+1}, \Upsilon_{t+1}\right) - f\left(\eta_t, G_t, a_{1,t}, \Upsilon_t\right) \le \frac{\rho}{2m}\sum_{i=1}^{m}\left(\kappa_{4,i,t}^2\left(\eta_{x,t+1}-\eta_{x,t}\right)^2 + \kappa_{5,i,t}^2\left(\eta_{y,t+1}-\eta_{y,t}\right)^2 + \kappa_{6,i,t}^2\left(\eta_{z,t+1}-\eta_{z,t}\right)^2\right) \\
&+\frac{\rho}{2m}\sum_{i=1}^{m}\left(\eta_{x,t}\left(G_{x,t+1}-G_{x,t}\right)^2 + \eta_{y,t}\left(G_{y,t+1}-G_{y,t}\right)^2 + \eta_{z,t}\left(G_{z,t+1}-G_{z,t}\right)^2\right)^2 + \frac{1}{2m}\sum_{i=1}^{m}\left(1+\rho\kappa_{2,i,t}^2\right)\left(a_{1,t+1}-a_{1,t}\right)^2 \\
&+\frac{2}{\tau}\left(\tau-1\right)^2\rho\frac{1}{m}\sum_{i=1}^{m}\left(\Phi_i\left(a_{t+1}, G_{t+1}, \eta_{t+1}\right) - \Phi_i\left(a_t, G_t, \eta_t\right)\right)^2 + 2\frac{1}{\rho\tau}\left(\frac{1}{m}\sum_{i=1}^{m}\left(\frac{1}{\kappa_{2,i,t+1}}\left(a_{1,t+1}+\kappa_{1,i,t+1}\right) - \frac{1}{\kappa_{2,i,t}}\left(a_{1,t}+\kappa_{1,i,t}\right)\right)\right)^2 \le 0, \qquad \text{(S11)} \\
&\Rightarrow \rho \le 0, \eta_{x,t} \ge 0, \eta_{y,t} \ge 0, \eta_{z,t} \ge 0, \frac{2}{\tau}\left(\tau-1\right)^2\rho \le 0, \frac{1}{\rho\tau} \le 0, \\
&\Rightarrow \rho \le 0, \eta_{x,t} \ge 0, \eta_{y,t} \ge 0, \eta_{z,t} \ge 0, \tau \ge 0.
\end{aligned}
$$

Hence, (S5a) and (S6a) are fulfilled, which demonstrates that (23) is non-increasing in this case. After (t+1)-*th* iteration, (23) can be reformulated as:

$$
f\left(\eta_{t+1}, G_{t+1}, a_{1,t+1}, \Upsilon_{t+1}\right) = \frac{1}{2m}\sum_{i=1}^{m}\left\|B_i - \hat{C}_i\right\|_2^2 + \frac{1}{m}\sum_{i=1}^{m}\left\langle\Psi_i\left(a_{1,t+1}, G_{t+1}, \eta_{t+1}\right), \Upsilon_{t+1}\right\rangle + \frac{1}{2m}\sum_{i=1}^{m}\rho\left\|\Psi_i\left(a_{1,t+1}, G_{t+1}, \eta_{t+1}\right)\right\|_2^2. \qquad \text{(S12)}
$$

By substituting (S3) into (S11), we can obtain:

$$
f\left(\eta_{t+1}, G_{t+1}, a_{1,t+1}, \Upsilon_{t+1}\right) = \frac{1}{2m}\sum_{i=1}^{m}\left\|B_i - \hat{C}_i\right\|_2^2 + \frac{\left(2\tau-1\right)\rho}{2}\frac{1}{m}\sum_{i=1}^{m}\left(\Phi_i\left(a_{1,t+1}, G_{t+1}, \eta_{t+1}\right)\right)^2 - \frac{1}{m}\sum_{i=1}^{m}\frac{1}{\kappa_{2,i,t+1}}\left(a_{1,t+1}+\kappa_{1,i,t+1}\right). \qquad \text{(S13)}
$$

With (S5b) and (S13), (S6b) is fulfilled, i.e., (23) is lower-bounded. Hence, *Lamma* 2 stands, making Step 2 complete. To sum up, as per the aforementioned deductions, with the implementation of Steps 1 through 2, AMPC's convergence can be established with certainty in theory.